Article type: Full Paper

Multifunctional Beam Manipulation at Telecommunication Wavelengths Enabled by an All-Dielectric Metasurface Doublet

Changyi Zhou, Woo-Bin Lee, Chul-Soon Park, Song Gao, Duk-Yong Choi[*], and Sang-Shin Lee[*]

Mr. C. Zhou, Mr. W.-B. Lee, Dr. S. Gao, Prof. S.-S. Lee

Department of Electronic Engineering

Kwangwoon University

Seoul, 01897, South Korea

Mr. C. Zhou, Mr. W.-B. Lee, Dr. C.-S. Park, Prof. S.-S. Lee

Nano Device Application Center

Kwangwoon University

Seoul, 01897, South Korea

Dr. S. Gao

School of Information Science and Engineering

University of Jinan

Jinan, Shandong, 250022, China

Prof. D.-Y. Choi

Laser Physics Centre

Research School of Physics

Australian National University

Canberra, ACT 2601, Australia

Prof. D.-Y. Choi

College of Information Science and Technology

Jinan University

Guangzhou, Guangdong, 510632, China

E-mail: duk.choi@anu.edu.au

E-mail: slee@kw.ac.kr

Keywords: metasurface doublet; multifunction; dielectric; telecommunication wavelength; polarization-controlled

Abstract: Multifunctional metasurfaces, which are planar devices featuring diverse functionalities, have attracted tremendous attention as they enable highly dense integration and miniaturization of photonic devices. Previous approaches based on spatial/spectral multiplexing of meta-atoms on single metasurfaces are supposed to be inevitably limited in their functional diversity. An additional degree of freedom for design, achieved by cascading multiple metasurfaces into a single metasystem, promotes new combinations of functions that cannot be achieved with single-layered metasurfaces. In this study, an all-dielectric metasurface doublet (MD) was developed and implemented by vertically concatenating two arrays of rectangular nanoresonators on either side of a quartz substrate, in which distinct phase profiles were encoded for transverse magnetic and transverse electric polarized light. Multifunctional beam manipulation with concurrent increased beam deflection, beam reduction, and polarizing beam splitting was achieved at telecommunication wavelengths near 1550 nm. The MD was accurately created via lithographical nanofabrication, thus eliminating the extremely demanding post-fabrication alignment. The proposed multifunctional metasurface is highly anticipated to expedite the development of advanced

technologies for large-scale photonic integration, optical metrology, light detection and ranging, spectroscopy, and optical processing.

Optical components, including Risley prisms, lenses, spherical mirrors, and polarizing beam splitters, have been extensively used to construct light detection and ranging (LiDAR) systems,[1-3] afocal telescopes,[4] laser communication systems,[5] and quantum computing systems.[6,7] To reduce the lens weight and volume, a diffraction-based Fresnel optics configuration was realized by tailoring either the phase or amplitude of the propagating light.[8] However, its application has been hindered by the limited controllability of light and complex multilevel lithographic fabrication processes.[9,10] Nanostructured metasurfaces incorporating subwavelength nanoresonators, developed as vital substitutes for conventional Fresnel optics schemes, enable more facile wavefront shaping than the conventional refractive/diffractive elements,[11-15] promoting the development of portable and wearable devices.[16-18] For instance, high-numerical-aperture flat metasurface lenses (metalenses) enabling diffraction-limited focusing at different wavelengths have been proposed.[16] It was experimentally proven that a metalens with a diameter of 240 µm providing magnifications as high as 170 could offer image quality on par with that achievable using state-of-the-art commercial bulky objectives. However, comatic or chromatic aberration hampers the integration of metalenses from providing off-axis or full-color imaging. Recently, a comatic

4

aberration compensated metalens, which consists of dielectric nanoring structures of different heights fabricated by 3D printing, has been demonstrated for wide-angle imaging.[19] An ultrathin metalens based on the scheme of hybridizing nanoring structures into a single layer could lead to a wide field of view as well as low-cost mass production. Besides, cascaded metasurfaces are known to be useful for mitigating chromatic aberration.[20,21] It is hence asserted the scheme of cascading can be leveraged to control the phase, amplitude, and polarization of electromagnetic waves simultaneously. The multi-layer stacking scheme enables the mitigation of issues such as insufficient beam manipulation, image quality degradation, and undesirable diffraction orders, by spatially multiplexing resonators on the same metasurface. In particular, optical metasystems consisting of two or more metasurfaces have mainly been exploited to produce compact devices acting as retroreflectors,[22] spectrometers,[23] hyperspectral imagers,[24] and optical planar cameras.[25] While the aforementioned metasurfaces were developed to serve single functions, multifunctional metasurfaces that can perform multiple tasks have attracted considerable interest owing to their potential use as multifocal or achromatic lenses,[26-28] metadevices serving distinct wave-manipulation functionalities,[29-35] imaging systems,[36-38] nonlinear coding metasurfaces,[39-41] and vector vortex beam (VVB) generators.[42,43] For instance, metasurfaces in the visible or millimeter-wave regime have been applied to implement VVB generators leading to vortex beams with different topological charges, with the assistance of

unit cells consisting of multiple nanoblocks/layers with different geometrical parameters.[42,43]

Meanwhile, single-layered metasurfaces are inherently limited in terms of functional diversity.

In this paper, we propose and describe the experimental realization of an all-dielectric metasurface doublet (MD) that enables multifunctional beam manipulation in the near-infrared (NIR) regime, including increased beam deflection, beam reduction, and polarizing beam splitting. For the nanoresonators, the optical transfer characteristics can be polarization-tailored in terms of the phase and amplitude to engineer the phase profiles for the MD, which are distinct for transverse electric (TE) and transverse magnetic (TM) polarization. The concatenation of metasurfaces could enable a suite of new functionalities that may not be achievable using single metasurfaces. A series of simulations was rigorously executed to design and characterize the proposed MD. Two disparate elemental metasurfaces were precisely created and aligned on either side of a thin glass substrate, with reference to the corresponding alignment markers inscribed on each side. From the perspective of alignment during fabrication, such an MD device is preferable to a device consisting of two separate metasurfaces.[25] For the created MD, incident light can be separated into two orthogonally polarized beams, where the TE-polarized beam travels straight, following the incident angle, whereas the TM-polarized beam is efficiently routed by an angle equivalent to three times the incident angle. The beam width of the deflected TM-polarized light shrinks by

6

half. In addition, a broad working wavelength range of 1500–1600 nm was observed. In view of the performance achieved at telecommunication wavelengths, it is incontrovertible that the proposed metasurface device could play a pivotal role in establishing free-space optical communications, optical interconnections, and spatially resolved optical sensors.[44]

Figure 1a shows a schematic of the proposed multifunctional MD operating in the NIR regime, where the TE- and TM-polarized light beams are oriented along the *x*- and *y*-axes, respectively. An incident TM-polarized beam deflects to assume an increased propagation angle, while the width of the outgoing beam decreases. The deflection angle θ_{out} is given by $\theta_{out} = M \times \theta_{in}$, where *M* is the magnification factor and θ_{in} is the incident angle. Simultaneously, the TE-polarized beam travels straight through the MD, facilitating the splitting of an orthogonally polarized beam. In other words, the proposed device can concurrently serve three functions at telecommunication wavelengths in a flat planar platform, with increased beam deflection and efficient beam reduction in tandem with polarizing beam splitting. A pair of subwavelength gratings, including a one-dimensional (1D) array of rectangular dielectric resonators (RDRs) in hydrogenated amorphous silicon (a-Si:H), was created on a 902-μm-thick quartz substrate. The two grating structures were intended to act as cascaded metasurfaces (MS1 and MS2). RDRs are known not to be vulnerable to ohmic loss in connection with metallic structures, making the dielectric based metasurface more efficient than plasmonic-based metasurfaces.[45,46] As depicted in **Figure**

1a, the proposed device has a footprint of $L_1 = 400$ μm by $L_2 = 250$ μm, where each RDR element has dimensions of w (width), L_2 (length), and h (height). Considering that the device is intended to work near $\lambda = 1550$ nm, 16 RDRs each with $h = 930$ nm (~0.6 λ) and $L_2 = 250$ μm were arranged with a period of $p = 800$ nm along the y-axis, while w ranged from 150 nm to 366 nm. For an RDR with $w = 366$ nm, the simulated magnetic field intensity in response to a normally incident TM-polarized beam in the inset of **Figure 1**a indicates that light is mainly confined inside the high-refractive-index RDR.[47] The device was prepared using conventional electron beam (e-beam) lithography and plasma etching. **Figure 1**b shows a set of scanning electron microscope (SEM) images of the fabricated device on a 902-μm-thick quartz substrate, with MS1 and MS2 patterns on the front and back sides thereof (see the Experimental Section and Section S1 in the Supporting Information for details).

Multiple functions achievable using the proposed MD can be realized by selectively triggering the phase profiles contingent on incident light polarization. To implement the MD, as depicted in **Figure 2**a, a conventional doublet lens incorporating two optical surfaces (OS1 and OS2) was firstly envisioned and devised to increase the beam deflection and beam reduction in the case of TM-polarized light. The doublet lens was elaborately built with the assistance of 3D optical engineering and design software, LightTools (Synopsys, USA). The first surface, OS1, was particularly designed to minimize the spot size so that incident beams with slightly different angles could be spatially segregated prior to reaching the second

8

surface, OS2, which controls the beam deflection angle. A doublet lens is utilized to manipulate the incident light, as in an optics configuration allowing for an angular magnification of M, where a convex lens with a focal length f is tethered to a concave lens with a focal length of f/M.[48,49] The equation for defining an aspheric contour in the yz-plane is $z = \dfrac{C \cdot y^2}{1 + \sqrt{1 - (1 + k)C^2 y^2}}$, where C and k represent the curvature and conic constant, respectively.[50] In accordance with the objective of deflecting the incident light such that the propagation angle of the outgoing beam is increased by a factor of three compared to the incident angle, the contours for the designed OS1 and OS2 were determined to be

$z_1 = \dfrac{0.29 y^2}{1 + \sqrt{1 + 3.1 \times (0.29)^2 y^2}}$ and $z_2 = \dfrac{0.87 y^2}{1 + \sqrt{1 - (0.87)^2 y^2}}$, respectively. According to the design in **Figure 2**a, the doublet lens can be equivalently made by placing two flat sub-lenses on either side of a substrate. The phase profiles corresponding to OS1 and OS2 that are dictated by the above equations, denoted as φ_1(TM) and φ_2(TM), respectively, were derived by referring to the discretized sag S and are indicated by solid black lines in **Figures 2**b and **2**c[18,51] (detailed discussions regarding the phase profile calculation and doublet lens design can be found in Section S2 of the Supporting Information). **Figure 2**d shows the simulated phase change for the transmitted electric field for normally incident TM-polarized light, in parallel with the transmission of each unit cell made of RDRs. Owing to a high-index contrast between a-Si:H and the air, the RDRs can impart an entire 2π phase shift under sufficiently

9

high transmission.[52,53] For the selected RDRs, **Figure S3** implies that the imparted phase shift remains relatively constant, while the transmission decreases slightly with increasing θ_{in}. Thus, the constructed MD is guaranteed to work under obliquely incident light to a certain extent[54] (please see Section S3 in the Supporting Information for a detailed discussion).

Based on the method of devising a metalens,[11,12,16,17] OS1 and OS2 were successfully replaced with MS1 and MS2, in which selected RDRs were arranged to emulate the phase profiles represented by φ_1(TM) and φ_2(TM), respectively. The targeted MD was consequently established by precisely aligning and mounting MS1 and MS2 on both sides of a substrate. The expansion of beam deflection mediated by the MD, which is approximately equal to that of the original doublet lens, can be controlled by tailoring the lens curvature. **Figure 2**e illustrates the operation mechanism of the proposed MD in terms of the ray-optical behavior in the TM-polarized case. An incident beam propagates obliquely in the *yz*-plane along the black arrows, then is sequentially bent inward by MS1 to arrive at MS2 after crossing the thin substrate. Due to the cooperation between the two metasurfaces, a TM-polarized beam is expected to deviate to assume an increased propagation angle, $\theta_{out} \approx M \times \theta_{in}$, while delivering a diminished beam width (please see Section S2 in the Supporting Information for a detailed discussion). In the TE-polarized case, the two metasurfaces are deemed to cause no phase gradient; therefore, the incoming wavefront undergoes no manipulation, as shown in **Figure 2**f. Consequently, the proposed MD can efficiently split an orthogonally polarized incident

beam into two individual beams depending on the polarization (please see Section S4 in the Supporting Information for details).

To validate the device performance, rigorous simulations were executed using commercial finite-difference time-domain software, FDTD Solutions (Lumerical, Canada). **Figure 3**a presents the relationship between θ_{out} and θ_{in}, alongside the calculated intensity transmission (T), reflection (R), and absorption (A). The beam deflection of TM-polarized light was explored by varying θ_{in} from 0° to 12°. The angular range of the deflected beam was predicted to increase up to 39.2°. Correspondingly, the span of the beam deflection could be as much as 78.4° in our symmetric MD. The designed device can yield beam deflection magnification corresponding to $M \approx 3$ with transmission of up to 82.9% (please see Section S5 in the Supporting Information for details). For the fabricated MD, the maximum angle of acceptance was observed to be 12°, beyond which the beam exiting MS1 was not fully accommodated by MS2. The angular range could be increased by enlarging the dimensions of the device, especially L_1, considering that the increased beam deflection occurs in the direction along L_1. The degraded transmission efficiency under oblique incidence is considered to be due to the increased absorption in the RDRs. The calculated electric field E_y distributions in the yz-plane for MS1 and MS2 upon illumination by a TM-polarized plane wave are given in **Figure 3**b. The incident beam is evidently bent inward by MS1 and routed outward by MS2 so that the deflection angle of the outgoing beam eventually becomes

11

equivalent to three times the incident angle. The a-Si:H RDRs affiliated with the MD may be treated as a truncated waveguide, working as a low-quality-factor Fabry-Pérot resonance, which is related to Fresnel reflections at either end of the waveguide.[27] Notably, the proposed MD can cause beam deflection corresponding to three times the incident angle, which can be flexibly controlled by manipulating φ_1(TM) and φ_2(TM). For TM-polarized light, we also explored a highly directional far-field profile, as shown in **Figure 3**c, in which the upper and lower two images portray the situations in the absence and presence of the MD, respectively. Considering the light trajectory with the MD in action, the $1/e^2$ beam width has noticeably shrunk. Regarding the beam reducer based on the proposed MD, the working distance is defined as the distance from MS1 to the position at which the size of the outgoing beam contracts by half compared with that of the incident beam. A cross-sectional profile of the emerging beam at z = 12 mm is plotted in **Figure 3**d. The beam widths for the on- and off-axis cases are the same at ~190 μm, implying that the width of the afocal TM-polarized beam decreases from 400 μm to 190 μm at the working distance. The proposed device can help decrease the beam size for both on- and off-axis incidence. Moreover, the 1D beam shaping initiated by the proposed MD helps circularize elliptically shaped beams as in the case of a cylindrical lens. Accordingly, this device is anticipated to be usable in applications in optical metrology, laser scanning, spectroscopy, laser diodes, acousto-optics, and optical processors.[55,56]

We experimentally investigated the optical response of the prepared MD. To assess the beam deflection enhancement provided by the MD, a tunable laser (Santec, ECL-200) served as a light source and a beam profiler was used as a detector (CINOGY, CinCam CMOS-1202), as shown in **Figure 4**a. Input light at $\lambda = 1550$ nm, whose polarization was adjusted using a polarization controller (KS Photonics, STPC), was collimated through a fiber collimator (PMPFX6, Thorlabs). The distance between the MD and sensing area inside the beam profiler is indicated by d. In the presence of the MD, the steering angle, θ_{st}, of the transmitted beam was recorded, when θ_{in} was scanned from 0° to 12° by rotating the MD. The deflection angle of the light is given by $\theta_{out} = \theta_{st} + \theta_{in}$, as described in the Method section. The transfer characteristics of the proposed MD for the increased deflection angle are depicted in **Figure 4**b. The slopes of the fitting lines corresponding to the measurement and simulation results are 3.55 and 3.25, respectively. Both the mean values and error bars related to the standard deviation were obtained from multiple measurements. Owing to its limited sensing area, the beam profiler was simultaneously displaced to capture the beam while altering θ_{in}. Several beam profiles were separately captured at $d = 35.6$ mm and are presented in **Figure 4**c.

Polarizing beam splitters based on metasurfaces are known to serve as integral platforms in the implementation of various polarization optics.[57-61] The proposed MD is anticipated to act as a planar polarizing beam splitter, mimicking a Rochon prism, which helps decompose

and route an arbitrarily polarized beam into two orthogonally polarized beams. The TE-polarized component remains on the same optical axis as the input, while the TM-polarized component deviates from it by an angle depending on θ_{in}. The beam that travels straight through is mainly useful for fulfilling the alignment of subsequent optical components in an optical system. Provided that a plane wave impinges upon the MD at an angle of 2°, carrying both TE and TM polarizations, the calculated far-field intensities, proportional to $|E_y|^2$, were individually normalized and are plotted in **Figures 5**a and **5**b, respectively. The TE-polarized beam continues to propagate in the same direction as θ_{in}, whereas the TM-polarized beam deflects toward another direction, corresponding to three times θ_{in}. The insets in the figures display the observed far-field profiles for the TE and TM cases. The resulting intensity as a function of θ_{out} is shown alongside the beam profile. For the transmitted TE and deflected TM beams, there is a decent correlation between the overall measured and simulated outcomes. However, the small angular discrepancy in conjunction with the imperfect beam splitting can be understood, considering that the light beam emanating from the fiber collimator (PMPFX6, Thorlabs) was about 500 μm in diameter, which was larger than the footprint of the fabricated MD sample (L_1 = 400 μm by L_2 = 250 μm). Thus, part of the incident beam outside of the MD was transmitted via the MD without undergoing the manipulation mediated by the metasurfaces, unintentionally leaking into and interfering with the output beam. In addition, the imperfect beam splitting could be ascribable

to fabrication errors, such as surface/edge roughness of the RDRs, discrepancies between the realized and designed structural parameters, and misalignment between the RDRs adopted for MS1 and MS2 on separate layers.[61-63] More importantly, the split angle between the two beams could readily be altered by properly choosing the incident angle ($\theta_{st} = (M - 1) \times \theta_{in} \approx 2\theta_{in}$). It is expected that a polarizing beam splitter utilizing the proposed miniatured MD could be applied in a versatile manner to implement integrated polarization optics, information security, and imaging.

As the proposed all-dielectric MD is anticipated to act as an integral component in the NIR regime, three wavelengths (1500, 1550, and 1600 nm) were utilized in the numerical simulations to validate the MD performance. The far-field light intensities proportional to $|E_y|^2$ are shown in **Figure 6**a, where incoming light is assumed to be TM-polarized for $\theta_{in} = 2°$. Accordingly, the beam deflection facilitated by the MD for each wavelength was experimentally confirmed. The beams captured by a beam profiler are displayed in **Figure 6**c and were appropriately fitted with a Gaussian distribution, as plotted in **Figure 6**b. The deflection angle and full width at half-maximum (FWHM) in response to the three wavelengths are summarized in Table 1. The deflected beam for the MD exhibits a slight angular shift while retaining nearly the same FWHM, leading to a wide working wavelength range. The spectral bandwidth of the dielectric metasurface could be broadened by using more layers.[64] A 100 nm spectral bandwidth in the NIR regime enables the proposed MD to

15

be applied in free-space optical communications[65] and military and civilian networks.[66]

Moreover, the proposed device could potentially be integrated with a solid-state optical

phased array chip to help establish a nonmechanical LiDAR module featuring enhanced

angular beam steering.[67,68]

The demonstrated MD is believed to be suitable for application to ultra-compact optical

systems. Its footprint can be increased from the sub-millimeter scale to several centimeters if

needed.[69-71] The tolerance for the thickness of the substrate supporting the two metasurfaces

was controlled within 5 μm. Regarding its compatibility with conventional microfabrication

techniques, the MD can readily be integrated into microelectromechanical systems to build

metasurface-based micro-optoelectromechanical systems[72,73] for tunable beam steering,

providing advantages such as fast tuning speed, small mechanical noise, and easy assembly.

Compared to a gradient metasurface enabling beam deflection[74,75] the demonstrated MD

features advanced performance in terms of the increased deflection angle, reduced beam size,

and controlled divergence angle (please see Section S6 in the Supporting Information for

details). The beam deflection achieved using the MD can be further improved by

manipulating the phase profiles derived from the doublet lens. For example, an MD rendering

beam deflection according to $M = 10$ can be attained by properly arranging the RDRs

corresponding to MS1 and MS2 (please see Section S7 in the Supporting Information for

details). However, there is a trade-off between the beam collimation and beam deflection.

The divergence angle should be increased in accordance with the amplification of deflection angle, which could be resolved by vertically stacking additional lenses.[48,76,77] Moreover, by replacing the uniformly long RDRs with polarization-dependent 2D nanoposts, which are popularly used for metasurface devices, an unprecedented MD could be developed to enhance the device efficiency and accommodate other prominent functions such as lens focusing, vortex beam generation, and holograms.[27-30,32,33]

In this work, an all-dielectric MD enabling multifunctional beam manipulation in the NIR band was presented to emulate the functions of optical components such as Risley prisms, cylindrical lenses, and polarizing beam splitters (please see Section S8 in the Supporting Information). The MD took advantage of 16 a-Si:H RDRs, allowing for polarization-controlled phases, to produce two metasurfaces on either side of a substrate. The MD was encoded with a phase profile that leads to a doublet lens for TM-polarized light and a plain substrate entailing no phase gradient for the TE-polarized case. Numerical simulations were executed to design and analyze the device. Each pair of vertically cascaded metasurfaces was patterned on a quartz substrate by referring to the alignment markers on either side using a transmission optical microscope. For the fabricated MD, amplified beam deflection in conjunction with polarizing beam splitting was verified within the spectral band from 1500 nm to 1600 nm. It is evident that the proposed scheme can be actively leveraged to

17

incorporate a set of bulk optics components into a single, ultra-thin device, paving the way for highly integrated compact photonics applications.

Experimental Section

Nanofabrication: MS1 and MS2, which constituted the MD, were formed on either side of a 902-µm-thick quartz substrate. The substrate was first cleaned with acetone/isopropyl alcohol/deionized water to promote adhesion between the glass substrate and a-Si:H layers. A 930-nm-thick layer of a-Si:H film was deposited on each side of the substrate using plasma-enhanced chemical vapor deposition (Plasmalab 100 from Oxford) under the optimal conditions derived in a previous study.[78] Then, MS1 was patterned on one side, followed by patterning of MS2 on the other side, as illustrated in **Figure S1**. An electron beam resist (ZEP520A from Zeon Chemicals) was spin-coated onto the substrate, and a thin layer of e-spacer 300Z (Showa Denko) was introduced to prevent charging during the subsequent e-beam lithography. The metasurface patterns and alignment marks were written on the resist via e-beam lithography (Raith150 EBL), accompanied by subsequent development (ZED-N50). A 60-nm-thick layer of aluminum was deposited by e-beam evaporation (Temescal BJD-2000) on the surface and patterned by lifting off the resist in a solvent (ZDMAC from Zeon Co.). The patterned aluminum was then used as the hard mask in dry

etching to transfer the designed pattern onto the underlying a-Si:H layer through fluorine-based inductively coupled plasma-reactive ion etching (Oxford Plasmalab System 100). The etching conditions were optimized to ensure a highly vertical profile for the a-Si:H RDRs. Finally, wet etching was performed to remove the residual aluminum etch mask. To place MS1 and MS2 precisely across the 902-μm-thick substrate, the relative displacement between the two alignment markers inscribed on either side was determined using a transmission optical microscope to indicate the positions of MS1 and MS2. Further details regarding the fabrication process are provided in Section S1 in the Supporting Information.

Measurement procedure: The setup and procedure used to characterize the completed MD devices are depicted in **Figure 4**a. The steering angle, θ_{st}, pertaining to the MD was measured when θ_{in} was scanned from 0° to 12° by manual rotation. When the MD was rotated counterclockwise, the beam was deemed to deflect toward the negative *y*-direction. The deflection angle was obtained as $\theta_{out} = \theta_{st} + \theta_{in}$, where θ_{st} was observed by moving the beam profiler along the *z*-direction. Positions P_0, P_1, and P_2 were recorded to determine θ_{st} as well as the distance, *d*, between the MD and the sensing area of the beam profiler. The wavelength of the output light from a tunable laser was checked beforehand with an optical spectrum analyzer (Anritsu, MS9710B). We used a polarization-maintaining fiber to prevent any polarization instabilities during the measurements.

Supporting Information

Supporting Information is available from the Wiley Online Library or from the author.

Acknowledgements

Received: ((will be filled in by the editorial staff))

Revised: ((will be filled in by the editorial staff))

Published online: ((will be filled in by the editorial staff))

REFERENCES

[1] Z. Pan, P. Hartzell, C. Glennie, *IEEE Geosci. Remote Sens. Lett.* **2017**, *14*, 1418.

[2] A. Li, X. Liu, W. Sun, *Opt. Express* **2017**, *25*, 7677.

[3] A. Li, W. Sun, W. Yi, Q. Zuo, *Opt. Express* **2016**, *24*, 12840.

[4] A. Gómez-Vieyra, A. Dubra, D. Malacara-Hernández, D. R. Williams, *Opt. Express* **2009**, *17*, 18906.

[5] R. Prevedel, P. Walther, F. Tiefenbacher, P. Bohi, R. Kaltenbaek, T. Jennewein, A. Zeilinger, *Nature* **2007**, *445*, 65.

[6] T. B. Pittman, B. C. Jacobs, J. D. Franson, *Johns Hopkins Apl. Technical Digest* **2004**, *25*, 84.

[7] S. Barz., *J. Phys. At. Mol. Opt. Phys.* **2015**, *48*, 083001.

[8] X. Zheng, B. Jia, H. Lin, L. Qiu, D. Li, M. Gu, *Nat. Commun.* **2015**, *6*, 8433.

[9] G. Yoon, J. Jang, J. Mun, K. T. Nam, J. Rho, *Commun. Phys.* **2019**, *2*, 156.

[10] F. Capasso, *Nanophotonics* **2018**, *7*, 953.

[11] A. V. Kildishev, A. Boltasseva, V. M. Shalaev, *Science* **2013**, *339*, 1232009.

21

[12] L. Huang, X. Chen, H. Mühlenbernd, G. Li, B. Bai, Q. Tan, G. Jin, T. Zentgraf, S. Zhang, *Nano Lett.* **2012**, *12*, 5750.

[13] N. Yu, F. Capasso, *J. Lightwave Technol.* **2015**, *33*, 2344.

[14] P. Yu, J. Li, S. Zhang, Z. Jin, G. Schütz, C. W. Qiu, M. Hirscher, N. Liu, *Nano Lett.* **2018**, *18*, 4584.

[15] P. Lalanne, P. Chavel, *Laser Photonics Rev.* **2017**, *11*, 1600295.

[16] M. Khorasaninejad, W. T. Chen, R. C. Devlin, J. Oh, A. Y. Zhu, F. Capasso, *Science* **2016**, *352*, 1190.

[17] S. Colburn, A. Zhan, A. Majumdar, *Optica* **2018**, *5*, 825.

[18] S. M. Kamali, A. Arbabi, E. Arbabi, Y. Horie, A. Faraon, *Nat. Commun.* **2016**, *7*, 11618.

[19] C. Hao, S. Gao, Q. Ruan, Y. Feng, Y. Li, J. K. W. Yang, Z. Li, and C. W. Qiu, *Laser Photonics Rev.* **2020**, 2000017.

[20] Y. Zhou, I. I. Kravchenko, H. Wang, J. R. Nolen, G. Gu, J. Valentine, *Nano Lett.* **2018**, *18*, 7529.

[21] A. S. Backer, *Opt. Express* **2019**, *27*, 30308.

[22] A. Arbabi, E. Arbabi, Y. Horie, S. M. Kamali, A. Faraon, *Nat. Photonics* **2017**, *11*, 415.

22

[23] M. Faraji-Dana, E. Arbabi, A. Arbabi, S. M. Kamali, H. Kwon, A. Faraon, *Nat. Commun.* **2018**, *9*, 4196.

[24] M. Faraji-Dana, E. Arbabi, H. Kwon, S. M. Kamali, A. Arbabi, J. G. Bartholomew, A. Faraon, *ACS Photonics* **2019**, *6*, 2161.

[25] A. Arbabi, E. Arbabi, S. M. Kamali, Y. Horie, S. Han, A. Faraon, *Nat. Commun.* **2016**, *7*, 13682.

[26] E. Arbabi, A. Arbabi, S. M. Kamali, Y. Horie, A. Faraon, *Optica* **2016**, *3*, 628.

[27] S. Gao, C. S. Park, S. S. Lee, D. Y. Choi, *Adv. Opt. Mater.* **2019**, *7*, 1801337.

[28] S. Gao, C. S. Park, C. Zhou, S. S. Lee, D. Y. Choi, *Adv. Opt. Mater.* **2019**, *7*, 1900883.

[29] S. Boroviks, R. A. Deshpande, N. A. Mortensen, S. I. Bozhevolnyi, *ACS Photonics* **2014**, *5*, 1648.

[30] F. Ding, R. Deshpande, S. I. Bozhevolnyi, *Light Sci. Appl.* **2018**, *7*, 17178.

[31] Z. Shi, M. Khorasaninejad, Y.-W. Huang, C. Roques-Carmes, A. Y. Zhu, W. T. Chen, V. Sanjeev, Z.-W. Ding, M. Tamagnone, K. Chaudhary, R. C. Devlin, C. W. Qiu, F. Capasso, *Nano Lett.* **2018**, *18*, 2420.

[32] F. Ding, Y. Chen, Y. Yang, S. I. Bozhevolnyi, *Adv. Opt. Mater.* **2019**, 1900724.

23

[33] T. Cai, S. W. Tang, G. M. Wang, H. X. Xu, S. L. Sun, Q. He, L. Zhou, *Adv. Opt. Mater.* **2017**, *5*, 1600506.

[34] Q. Jiang, Y. Bao, F. Lin, X. Zhu, S. Zhang, Z. Fang, *Adv. Funct. Mater.*, **2018**, *28*, 1705503.

[35] Y. Chen, J. Gao, X. Yang, *Laser Photonics Rev.* **2018**, *12*, 1800198.

[36] F. Zhang, M. Pu, P. Gao, J. Jin, X. Li, Y. Guo, X. Ma, J. Luo, H. Yu, X. Luo, *Adv. Sci.* **2020**, 1903156.

[37] C. Schlickriede, N. Waterman, B. Reineke, P. Georgi, G. Li, S. Zhang, T. Zentgraf, *Adv. Mater.* **2018**, *8*, 1703843.

[38] D. Wen, J. J. Cadusch, J. Meng, K. B. Crozier, *Adv. Funct. Mater.* **2019**, 1906415.

[39] S. Liu, T. J. Cui, L. Zhang, Q. Xu, Q. Wang, X. Wan, J. Q. Gu, W. X. Tang, M. Qi, J. G. Han, W. L. Zhang, X. Y. Zhou, Q. Cheng, *Adv. Sci.* **2016**, *3*, 1600156.

[40] Y. Bao, Y. Yu, H. Xu, Q. Lin, Y. Wang, J. Li, Z. K. Zhou, X. H. Wang, *Adv. Funct. Mater.* **2018**, *28*, 1805306.

[41] X. G. Zhang, W. X. Tang, W. X. Jiang, G. D. Bai, J. Tang, L. Bai, C. W. Qiu, T. J. Cui, *Adv. Sci.* 2018, *5*, 1801028.

[42] Z. H. Jiang, L. Kang, T. Yue, H. X. Xu, Y. Yang, Z. Jin, C. Yu, W. Hong, D. H. Werner, C. W. Qiu, *Adv. Mater.* **2020**, *32*, 1903983.

[43] Y. Bao, J. Ni, C. W. Qiu, *Adv. Mater.* **2020**, *32*, 1905659.

[44] J. H. Park, J. C. Park, K. R. Lee, Y. K. Park, *Adv. Mater.* **2019**, *1903457*.

[45] M. Khorasaninejad, F. Aieta, P. Kanhaiya, M. A. Kats, P. Genevet, D. Rousso, F. Capasso, *Nano Lett.* **2015**, *15*, 5358.

[46] C. R. de Galarreta, I. Sinev, A. M. Alexeev, P. Trofimov, K. Ladutenko, S. G.-C. Carrillo, E. Gemo, A. Baldycheva, V. K. Nagareddy, J. Bertolotti, C. D. Wright, arXiv:1901.04955, **2019**.

[47] W. Liu, Z. Li, H. Cheng, C. Tang, J. Li, S. Zhang, S. Chen, J. Tian, *Adv. Mater.* **2018**, *30*, 1706368.

[48] G. Liu, Q. Lu, W. Guo, *OSA Continuum* **2019**, *2*, 1746.

[49] P. Belland, J. P. Crenn, *Appl. Opt.* **1982**, *21*, 522.

[50] C. Pruss, E. Garbusi, W. Osten, *Opt. Photonics News* **2008**, *19*, 24.

[51] L. S. Pedrotti, Presented at *Society of Photo-Optical Instrumentation Engineers*, Bellingham, WA, December 5, **2008**.

[52] V. R. Almeida, Q. Xu, C. A. Barrios, M. Lipson, *Opt. Lett.* **2004**, *29*, 1209.

[53] Z. Wang, T. Li, A. Soman, D. Mao, T. Kananen, T. Gu, *Nat. Commun.* **2019**, *10*, 3547.

[54] D. Lin, M. Melli, E. Poliakov, P. S. Hilaire, S. Dhuey, C. Peroz, S. Cabrini, M. Brongersma, M. Klug, *Sci. Rep.* **2017**, *7*, 2286.

[55] K. Achouri, C. Caloz, *Sci. Rep.* **2018**, *8*, 7549.

[56] G. Konstantinou, P. A. Kirkby, G. J. Evans, K. M. Naga Srinivas Nadella, V. A. Griffiths, J. E. Mitchell, R. A. Silver, *Opt. Express* **2016**, *24*, 6283.

[57] H. Wei, F. Callewaert, W. Hadibrata, V. Velev, Z. Liu, P. Kumar, K. Aydin, S. Krishnaswamy, *Adv. Opt. Mater.* **2019**, *7*, 1900513.

[58] X. Xie, M. Pu, K. Liu, X. Ma, X. Li, J. Yang, X. Luo, *Adv. Mater. Technol.* **2019**, *4*, 1900334.

[59] G. Yoon, D. Lee, K. T. Nam, J. Rho, *Sci. Rep.* **2018**, *8*, 9468.

[60] X. Zhang, R. Deng, F. Yang, C. Jiang, S. Xu, M. Li, *ACS Photonics* **2018**, *5*, 2997.

[61] B. Wang, F. Dong, H. Feng, D. Yang, Z. Song, L. Xu, W. Chu, Q. Gong, Y. Li, *ACS Photonics* **2018**, *5*, 1660.

[62] S. Gao, S. S. Lee, E. S. Kim, D. Y. Choi, *Nanoscale* **2018**, *10*, 12453.

[63] Q.-T. Li, F. Dong, B. Wang, F. Gan, J. Chen, Z. Song, L. Xu, W. Chu, Y.-F. Xiao, Q.

Gong, Y. Li, *Opt. Express* **2016**, *24*, 16309.

[64] A. Ranjbar, A. Grbic, *Phys. Rev. Appl.* **2019**, *11*, 054066.

[65] V. W. Chan, *J. Lightwave Technol.* **2006**, *24*, 4750.

[66] J. A. Ratches, *Ferroelectrics* **2006**, *342*, 183.

[67] J. Sun, E. Timurdogan, A. Yaacobi, E. S. Hosseini, M. R. Watts, *Nature* **2013**, *493*, 195.

[68] H. Ito, Y. Kusunoki, J. Maeda, D. Akiyama, N. Kodama, H. Abe, R. Tetsuya, T. Baba,

Optica **2020**, *7*, 47

[69] N. Bonod, *Nat. Mater.* **2015**, *14*, 664.

[70] N. O. Länk, R. Verre, P. Johansson, M. Käll. *Nano Lett.* **2017**, *17*, 3054.

[71] G. M. Akselrod, J. Huang, T. B. Hoang, P. T. Bowen, L. Su, D. R. Smith, M. H.

Mikkelsen, *Adv. Mater.* **2015**, *27*, 8028.

[72] E. Arbabi, A. Arbabi, S. M. Kamali, Y. Horie, M. Faraji-Dana, A. Faraon, *Nat.

Commun.* **2018**, *9*, 812.

[73] C. Errando-Herranz, N. L. Thomas, K. B. Gylfason, *Opt. Lett.* **2019**, *44*, 855.

[74] R. A. Aoni, M. Rahmani, L. Xu, K. Z. Kamali, A. Komar, J. Yan, D. Neshev, A. E. Miroshnichenko, *Sci. Rep.* **2019**, *9*, 6510.

[75] Z. Zhou, J. Li, R. Su, B. Yao, H. Fang, K. Li, L. Zhou, J. Liu, D. Stellinga, C. P. Reardon, T. F. Krauss, X. Wang, *ACS Photonics* **2017**, *4*, 544.

[76] M. Zohrabi, R. H. Cormack, J. T. Gopinath, *Opt. Express* **2016**, *24*, 23798.

[77] M. Zohrabi, W. Y. Lim, R. H. Cormack, O. D. Supekar, V. M. Bright, J. T. Gopinath, *Opt. Express* **2019**, *27*, 4404.

[78] X. Gai, D. Y. Choi, B. L. Davies, *Opt. Express* **2014**, *22*, 9948.
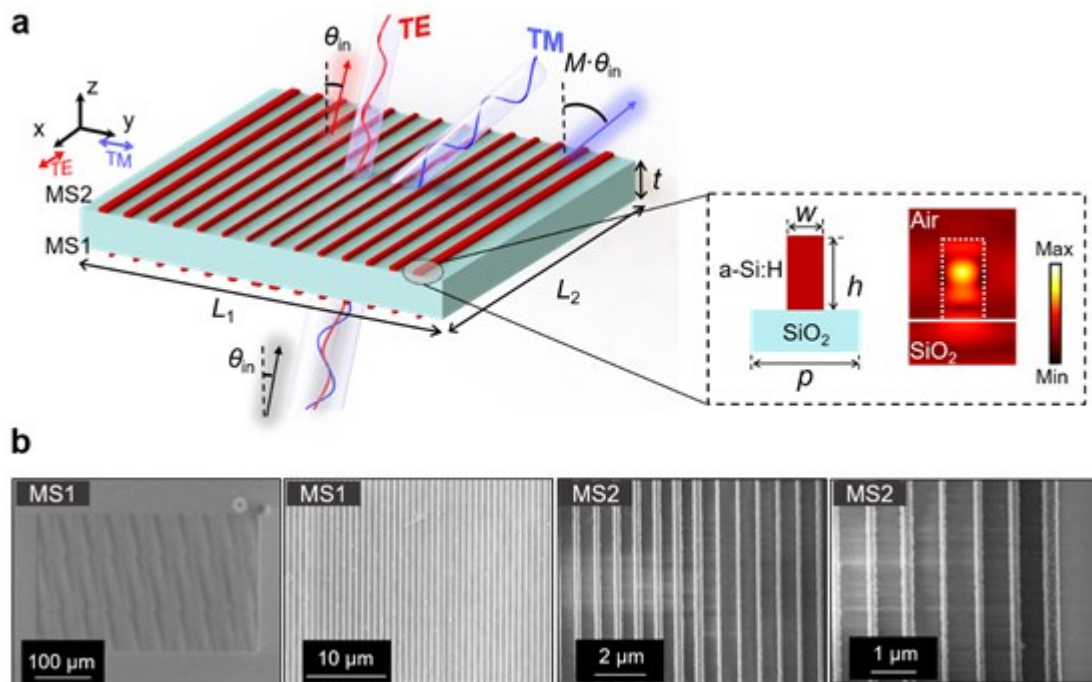
Figure 1 Monolithic MD. a) Schematic of the proposed multifunctional MD enabling beam deflection, beam reduction, and polarizing beam splitting. Inset: Configuration of a metasurface unit cell including an a-Si:H RDR formed on a quartz substrate. The optical fields are primarily confined to the RDR. b) Top-view SEM images of the fabricated MS1 and MS2 at different scales.
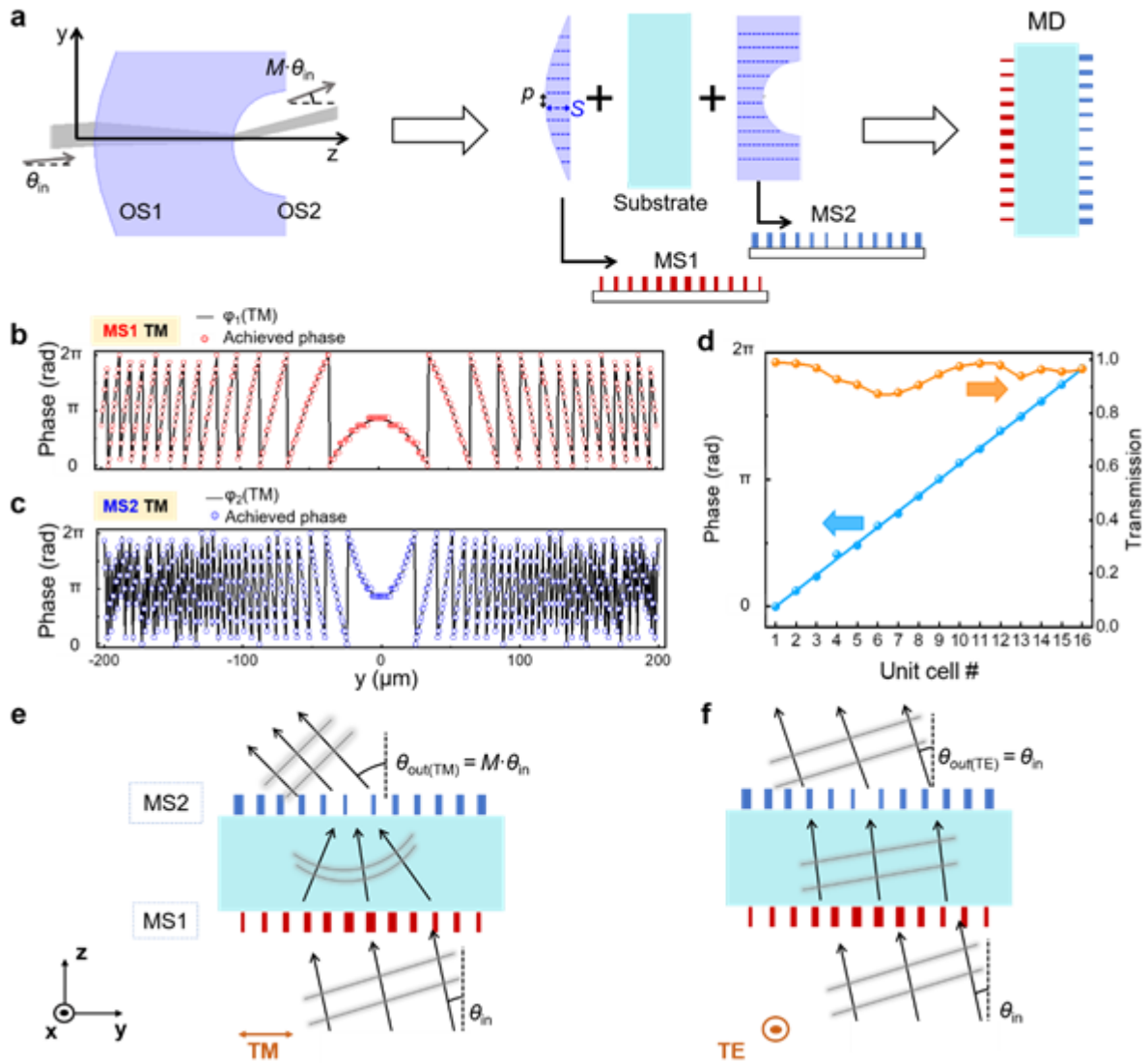
Figure 2 Design principle of the proposed all-dielectric MD. a) The development of the MD entailed the conversion of the constituents of the doublet lens, including OS1 and OS2, into their metasurface counterparts, which were put together. Desired and achieved phase profiles for b) MS1 and c) MS2 for TM-polarized light are provided as functions of the position of the MD. d) Phase shift and transmittance for the selected 16 RDRs at $\lambda = 1550$ nm for TM-polarized light. The TM and TE polarizations are along the e) width and f) length of the RDRs, respectively. Here, the operation mechanism underlying the MD is illustrated according to the ray-optic behavior, with light impinging upon MS1.
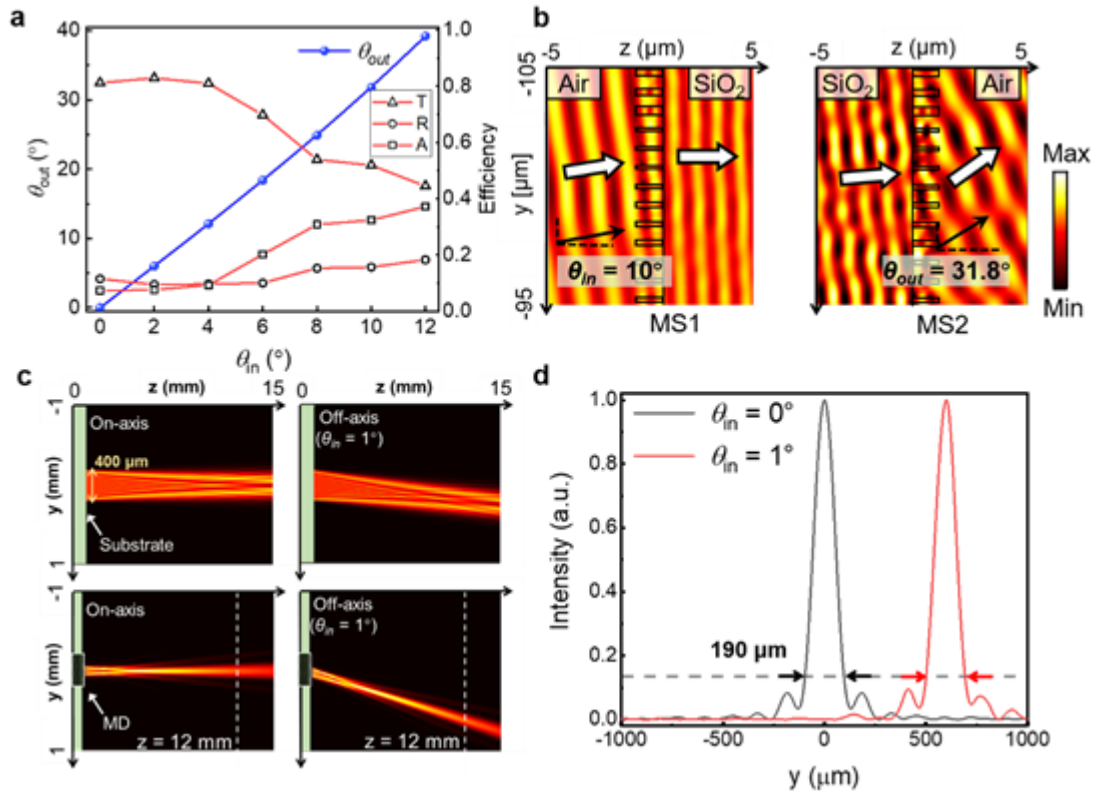
Figure 3 Numerical simulations for increased beam deflection and beam reduction. a) Calculated deflection angle in conjunction with the optical transmission, reflection, and absorption with the incident angle. b) Electric field distributions related to the E_y component under normal TM incidence for MS1 and MS2. c) Light intensity profiles of $|E_y|^2$ in the yz-plane depending on the presence of the MD: (top left) for an on-axis incident beam in the absence of the MD; (top right) for an off-axis incident beam in the absence of the MD; (bottom left) for an on-axis incident beam in the presence of the MD; (bottom right) for an off-axis incident beam in the presence of the MD. d) Light intensity profiles along the dashed line in c) at z = 12 mm, with the MD in action.

31
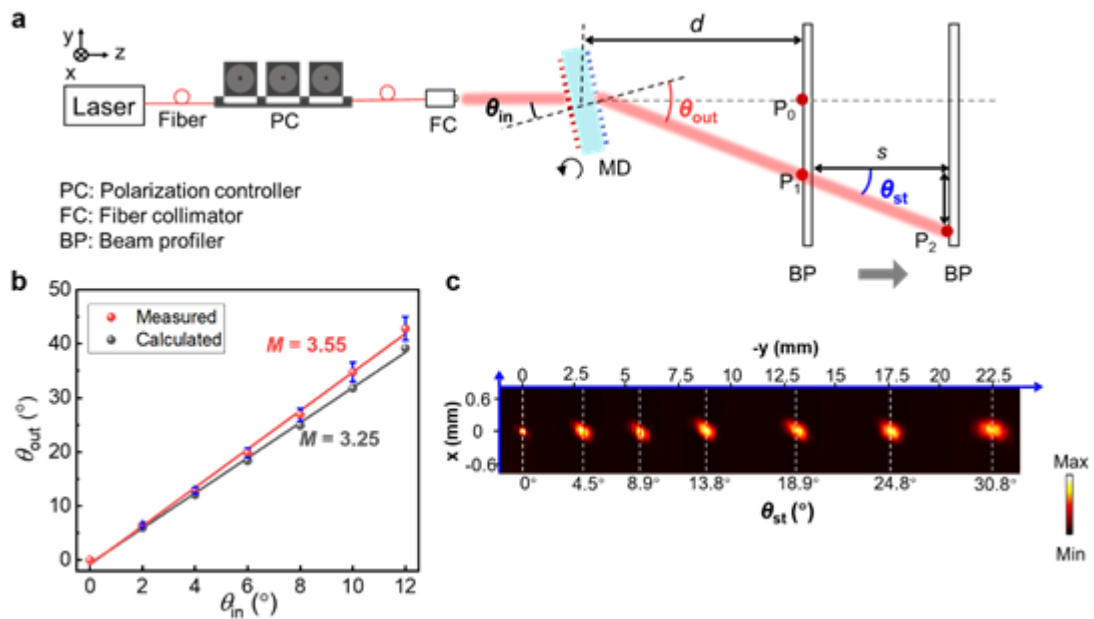
Figure 4 Experimental characterization for verifying increased beam deflection. a) Experimental setup for obtaining light intensity profiles in the yz-plane when the prepared MD was manually rotated. b) Demonstrated deflection angle of the proposed MD as a function of the incident angle. Both the mean value and standard deviation related to the error bars were obtained from multiple measurements. c) Captured beam profiles in the xy-plane in terms of θ_{st} at d = 35.6 mm.
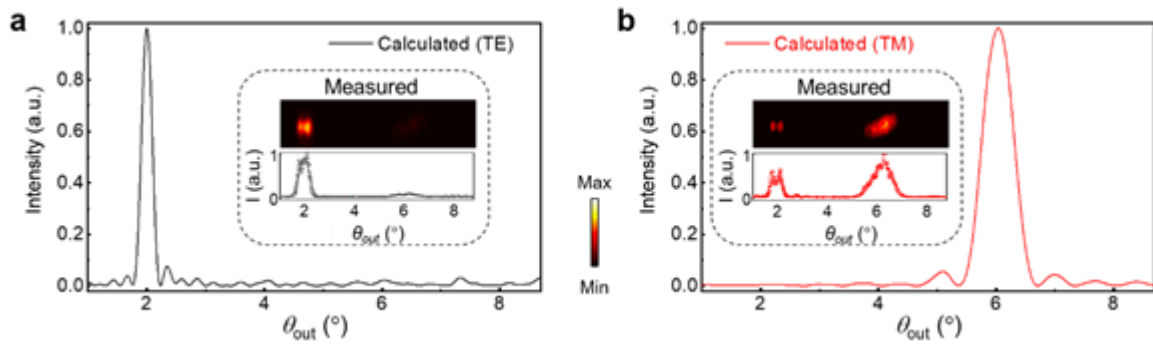
Figure 5 Demonstration of polarizing beam splitting. Calculated far-field intensity distributions for a) TE- and b) TM-polarized incident light with $\theta_{in} = 2°$. Insets: Captured beam profiles for the two orthogonal polarizations at $d = 28.0$ mm.
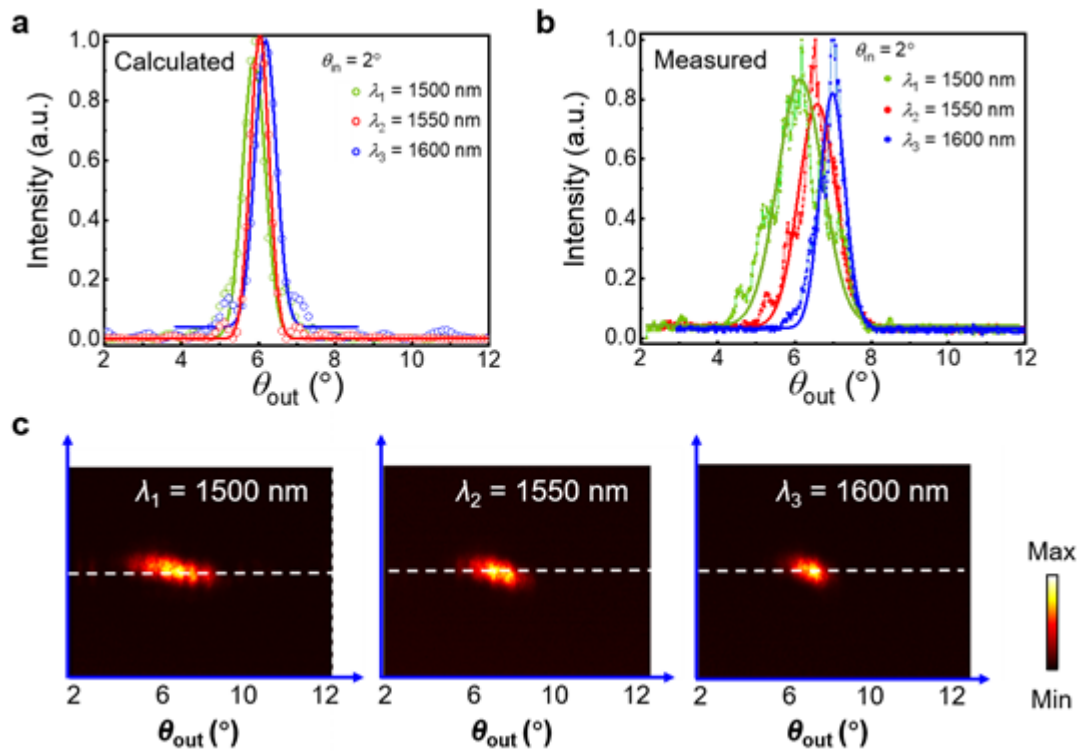
Figure 6 Beam deflection facilitated by the MD at telecommunication wavelengths. a) Calculated and b) measured far-field intensity distributions for the proposed MD with θ_{in} = 2° as observed at different wavelengths. The solid lines are the Gaussian fitted results. c) Captured beam profiles for the three wavelengths at d = 18.8 mm.

Table 1. Calculated and measured θ_{out} and FWHM according to wavelength.

Wavelength	Calculation		Measurement	
	θ_{out}	FWHM	θ_{out}	FWHM
λ_1 = 1500 nm	5.89°	0.70°	6.19°	0.83°
λ_2 = 1550 nm	6.04°	0.57°	6.54°	0.90°
λ_3 = 1600 nm	6.19°	0.66°	6.96°	0.77°

Metasurfaces enabling concurrent beam manipulation through compact design have attracted considerable attention in scientific research due to their great potentials in integrated photonic systems. In this report, we present and describe the experimental demonstration of an all-dielectric-based metasurface doublet providing multifunctional beam manipulation in the near-infrared regime, including increased beam deflection, beam reduction, and polarizing beam splitting.

Keywords: metasurface doublet; multifunction; dielectric; telecommunication wavelength; polarization-controlled

Changyi Zhou, Woo-Bin Lee, Chul-Soon Park, Song Gao, Duk-Yong Choi[*], and Sang-Shin Lee[*]

Multifunctional Beam Manipulation at Telecommunication Wavelengths Enabled by an All-Dielectric Metasurface Doublet